

Optomechanically induced stochastic resonance and chaos transfer between optical fields

Faraz Monifi^{1§}, Jing Zhang^{1,2,3}, Şahin Kaya Özdemir¹, Bo Peng^{1§§}, Yu-xi Liu^{3,4}, Fang Bo^{1,5},
Franco Nori^{6,7} & Lan Yang¹

Affiliations:

¹Department of Electrical and Systems Engineering, Washington University, St. Louis, MO 63130, USA

²Department of Automation, Tsinghua University, Beijing 100084, P. R. China

³Center for Quantum Information Science and Technology, TNList, Beijing 100084, P. R. China

⁴Institute of Microelectronics, Tsinghua University, Beijing 100084, P. R. China

⁵The MOE Key Laboratory of Weak Light Nonlinear Photonics, TEDA Applied Physics Institute and School of Physics, Nankai University, Tianjin 300457, China

⁶CEMS, RIKEN, Saitama 351-0198, Japan

⁷Physics Department, The University of Michigan, Ann Arbor, MI 48109-1040, USA

Current affiliations: [§]Department of Electrical and Computer Engineering, University of California, San Diego La Jolla, CA 92093-0407, USA. ^{§§}IBM Thomas J. Watson Research Center, Yorktown Heights, NY 10598, USA.

A. Experimental setup

An illustration of the setup used in our experiments is given in Fig. S1. An optical pump field, provided by a tunable External Cavity Laser Diode (ECLD) in the 1550 nm band, was first amplified using an erbium-doped fiber amplifier (EDFA), and then coupled into a fiber, using a

2-to-1 fiber coupler, together with a probe field provided by a tunable ECLD in the 980 nm band. A section of the fiber was tapered, to enable efficient coupling of the pump and probe fields into and out of a microtoroid resonator. The pump and probe fields in the transmitted signals were separated from each other using a wavelength division multiplexer (WDM) and then sent to two separate photodetectors (PDs). The electrical signals from the PDs were then fed to an oscilloscope, in order to monitor the time-domain behavior, and also to an electrical spectrum analyzer (ESA) to obtain the power spectra.

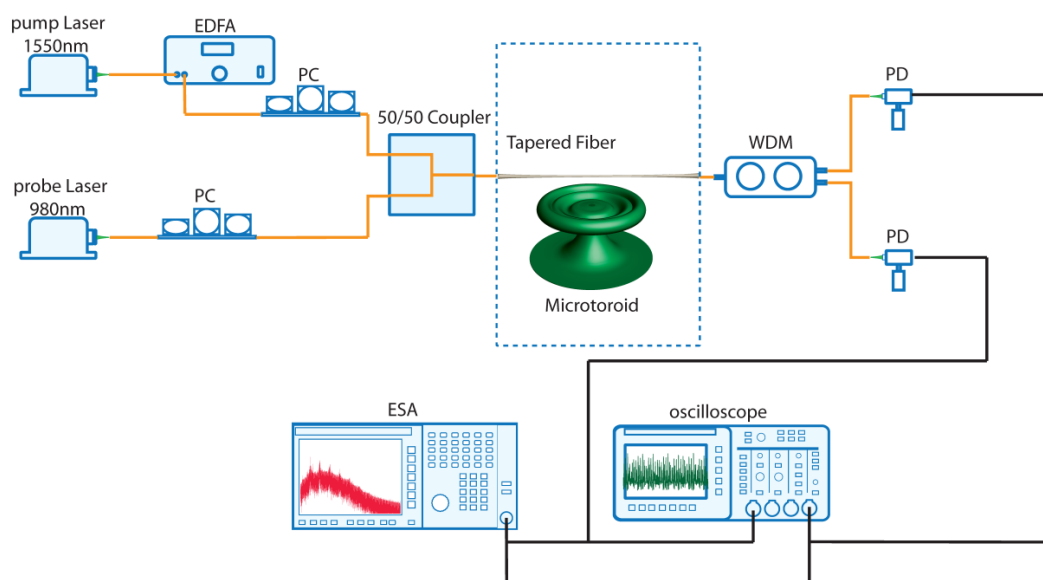


Figure S1. Schematic diagram of the experimental setup designed in a pump-and-probe configuration. The pump (1550 nm band) and the probe (980 nm band) fields were coupled into and out of a microtoroid resonator via the same tapered fiber in the same direction. EDFA: Erbium-doped fibre amplifier; PC: Polarization controller; WDM: Wavelength division multiplexer; PD: Photodetector; ESA: Electrical spectrum analyzer.

B. Spectral properties of pump and probe fields

Let us first assume that the intracavity pump and probe fields do not directly couple to each other, and that the probe and pump fields couple to the same mechanical mode of the microcavity with different coupling strengths. Below we show that in such a situation, the mechanical mode mediates an indirect coupling between the fields. The dynamical equation for the intracavity pump mode coupled to the mechanical mode of the cavity can be written as

$$\dot{a}_{\text{pump}} = -\left[\gamma_{\text{pump}} - i(\Delta_{\text{pump}} - g_{\text{pump}}X)\right]a_{\text{pump}} + i\kappa\varepsilon_{\text{pump}}(t), \quad (\text{S1})$$

where a_{pump} is the complex amplitude of the intracavity pump field, γ_{pump} is the damping rate of the cavity pump mode, $\varepsilon_{\text{pump}}(t)$ represents the amplitude of the input pump field, κ is the pump-resonator coupling rate, Δ_{pump} is the frequency detuning between the input pump field and the cavity resonance, X is the position of the mechanical mode coupled to a_{pump} , and g_{pump} is the strength of the optomechanical coupling between the optical pump field and the mechanical mode. This equation can be solved in the frequency-domain by using the Fourier transform as

$$a_{\text{pump}}(\omega) = \frac{-ig_{\text{pump}}}{i(\omega - \Delta_{\text{pump}}) + \gamma_{\text{pump}}} \int_{-\infty}^{+\infty} X(\omega - \omega_1) a_{\text{pump}}(\omega_1) d\omega_1 + \frac{i\kappa\varepsilon_{\text{pump}}(\omega)}{i(\omega - \Delta_{\text{pump}}) + \gamma_{\text{pump}}}, \quad (\text{S2})$$

where $a_{\text{pump}}(\omega)$, $X(\omega)$, and $\varepsilon_{\text{pump}}(\omega)$ are the Fourier transforms of the time-domain signals $a_{\text{pump}}(t)$, $X(t)$, and $\varepsilon_{\text{pump}}(t)$. Since the dynamics of the mechanical motion $X(t)$ is slow compared to that of the optical mode, we can replace the convolution term in the above equation by the product $a_{\text{pump}}(\omega)X(\omega)$, under the slowly-varying envelope approximation, which then leads to

$$\left[1 - \frac{-ig_{\text{pump}}}{i(\omega - \Delta_{\text{pump}}) + \gamma_{\text{pump}}} X(\omega) \right] a_{\text{pump}}(\omega) = \frac{-i\kappa\mathcal{E}_{\text{pump}}(\omega)}{i(\omega - \Delta_{\text{pump}}) + \gamma_{\text{pump}}}. \quad (\text{S3})$$

$X(\omega)$ is in general so small that we have $g_{\text{pump}}^2 |X(\omega)|^2 \ll (\omega - \Delta_{\text{pump}})^2 + \gamma_{\text{pump}}^2$. Then using the identity $1/(1-x) \approx 1+x$, for $x \ll 1$, we can re-write Eq. (S3) as

$$a_{\text{pump}}(\omega) = \left[1 + \frac{-ig_{\text{pump}}}{i(\omega - \Delta_{\text{pump}}) + \gamma_{\text{pump}}} X(\omega) \right] \frac{-i\kappa\mathcal{E}_{\text{pump}}(\omega)}{i(\omega - \Delta_{\text{pump}}) + \gamma_{\text{pump}}}. \quad (\text{S4})$$

By multiplying the above equation with its conjugate and dropping the linear term of $X(\omega)$, which is zero on average, we can obtain the relation between the spectrum $S_{\text{pump}}(\omega) = |a_{\text{pump}}(\omega)|^2$ of the optical mode a_{pump} and the spectrum of the mechanical motion $S_X(\omega) = |X(\omega)|^2$ as

$$S_{\text{pump}}(\omega) = \frac{\kappa^2 \mathcal{E}_{\text{pump}}^2}{\gamma_{\text{pump}}^2} \chi_{\text{pump}}(\omega) \left[1 + \frac{g_{\text{pump}}^2}{\gamma_{\text{pump}}^2} \chi_{\text{pump}}(\omega) S_X(\omega) \right], \quad (\text{S5})$$

where

$$\chi_{\text{pump}}(\omega) = \frac{\gamma_{\text{pump}}^2}{\gamma_{\text{pump}}^2 + (\omega - \Delta_{\text{pump}})^2} \quad (\text{S6})$$

is a susceptibility coefficient. If we further introduce the normalized spectrum

$$\tilde{S}_{\text{pump}}(\omega) = S_{\text{pump}}(\omega) - \frac{\kappa^2 \mathcal{E}_{\text{pump}}^2}{\gamma_{\text{pump}}^2} \chi_{\text{pump}}(\omega), \quad (\text{S7})$$

the above equation can be written as

$$\tilde{S}_{\text{pump}}(\omega) = \frac{\kappa^2 \varepsilon_{\text{pump}}^2 \mathcal{G}_{\text{pump}}^2}{\gamma_{\text{pump}}^4} \chi_{\text{pump}}^2(\omega) S_X(\omega). \quad (\text{S8})$$

We can obtain a similar equation by analyzing the spectrum of the optical mode a_{probe} coupled to the probe field as

$$\tilde{S}_{\text{probe}}(\omega) = \frac{\kappa^2 \varepsilon_{\text{probe}}^2 \mathcal{G}_{\text{probe}}^2}{\gamma_{\text{probe}}^4} \chi_{\text{probe}}^2(\omega) S_X(\omega), \quad (\text{S9})$$

where

$$\chi_{\text{probe}}(\omega) = \frac{\gamma_{\text{probe}}^2}{\gamma_{\text{probe}}^2 + (\omega - \Delta_{\text{probe}})^2}, \quad (\text{S10})$$

γ_{probe} is the damping rate of the cavity mode coupled to the probe field, $\varepsilon_{\text{probe}}(t)$ represents the amplitude of the input probe field, Δ_{probe} is the detuning between the input probe field and the cavity resonance, and g_{probe} is the coupling strength between the optical mode a_{probe} and the mechanical mode.

From Eqs. (S8) and (S9), we obtain the relation between the normalized spectra $\tilde{S}_{\text{pump}}(\omega)$ and $\tilde{S}_{\text{probe}}(\omega)$ as

$$\tilde{S}_{\text{probe}}(\omega) = G \frac{\chi_{\text{probe}}^2(\omega)}{\chi_{\text{pump}}^2(\omega)} \tilde{S}_{\text{pump}}(\omega), \quad (\text{S11})$$

where

$$G = \frac{\varepsilon_{\text{probe}}^2 \mathcal{G}_{\text{probe}}^2 \gamma_{\text{pump}}^4}{\varepsilon_{\text{pump}}^2 \mathcal{G}_{\text{pump}}^2 \gamma_{\text{probe}}^4}. \quad (\text{S12})$$

If we assume that the detunings and damping rates of the optical modes are close to each other, i.e., $\Delta_{\text{pump}} \approx \Delta_{\text{probe}}$ and $\gamma_{\text{pump}} \approx \gamma_{\text{probe}}$, we have $\chi_{\text{probe}}^2(\omega)/\chi_{\text{pump}}^2(\omega) \approx 1$, leading to

$$\tilde{S}_{\text{probe}}(\omega) \approx G \tilde{S}_{\text{pump}}(\omega). \quad (\text{S13})$$

This implies that the spectra of the pump and probe fields are correlated with each other. The correlation factor G is mainly determined by the optomechanical coupling strengths of the pump and the probe fields as well as the intensities of these fields. The relation between the spectra of the pump and probe signals shows that the optomechanical coupling strengths g_{pump} and g_{probe} of the pump and probe field to the excited mechanical mode determine how closely the probe field will follow the pump field. Clearly, these coupling strengths do not change the shape of the spectrum, and this is the reason why the probe signal follows the pump signal in the frequency domain and enters the chaotic regime via the same bifurcation route, despite the fact that they are far detuned from each other (Fig. 2c, 2d).

In our experiments, the mechanical motion was excited by the strong pump field, and the probe was chosen to have such a low power that it could not induce any mechanical oscillations. The large pump and probe detuning ensured that there is no direct coupling between them. The fact that both the pump and the probe are within the same resonator that sustains the mechanical oscillation naturally implies that both the pump and the probe are affected by the same mechanical oscillation with varying strengths, depending on how strongly they are coupled to the mechanical mode. The pump and probe spectra (Fig. S2) obtained in our experiments under these conditions agree well with the theoretical prediction given in Eq. (S13), in the sense that the spectra of the pump and the probe fields become correlated if they couple to the same mechanical mode. The slight differences in phase diagrams obtained in the experiments (Fig. 2a, 2b) imply that different coupling strengths of the pump and probe to the same mechanical mode,

due to the difference in their spatial overlaps with the mechanical mode, affect the trajectories and thus the phase diagrams.

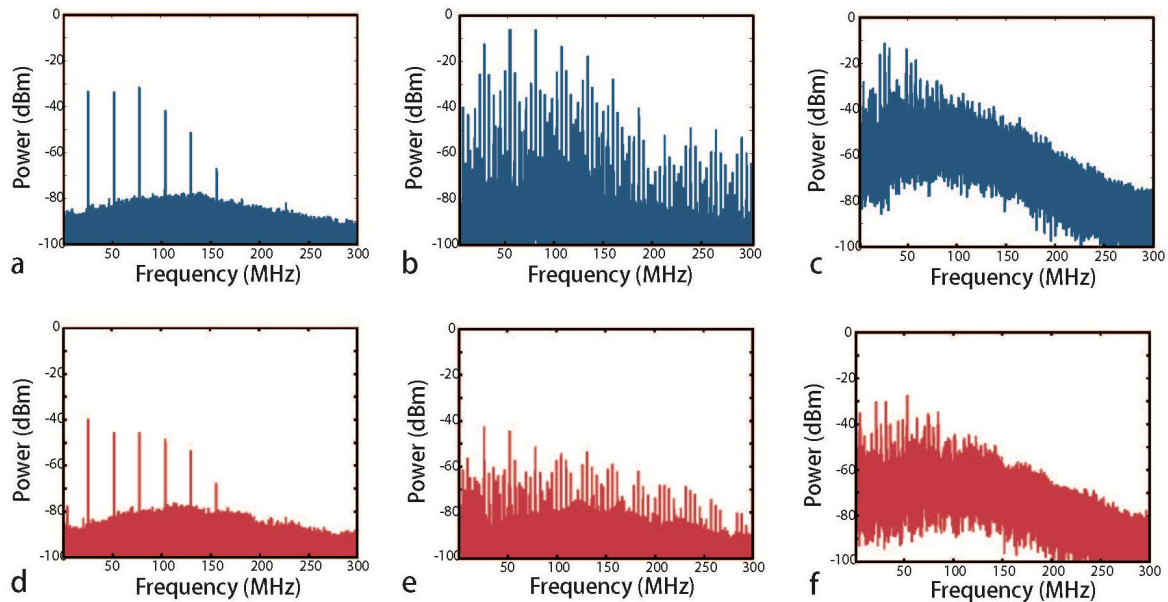


Figure S2. Experimentally-obtained power spectra for the pump and probe fields at various pump powers corresponding to (a,d) periodic, (b,e) quasi-periodic, and (c,f) chaotic regime. The spectra of the pump (a-c) and the probe (d-f) fields show similarities in these regimes.

C. Bifurcation analysis of the pump and probe fields

Here we consider the bifurcation process and determine the route to chaos for the pump and probe fields. In our experiments, we observed a mechanical mode with a frequency of around 26 MHz, and monitored the evolution of this mode as a function of the power of the input pump field. As shown in Fig. S3a, both the pump and probe fields experienced a period-doubling bifurcation as the input power of the pump field was increased: When the input pump power was

low, the spectra of the pump and probe fields showed a peak at around 26 MHz. When the input pump power was increased above a critical value, a second peak appeared just at half frequency of the main peak, i.e., ~ 13 MHz which corresponds to a period-doubling process. At higher powers, successive period-doubling events occurred, leading to peaks located at frequencies of $1/2^n$ -th of the main peak. For example, the second period-doubling bifurcation led to frequency peaks at 6.5 MHz for both the pump and the probe fields.

In Fig.S3b, we present the results of numerical simulations obtained by solving the following set of equations

$$\dot{a}_{\text{pump}} = -\left[\gamma_{\text{pump}} - i(\Delta_{\text{pump}} - g_{\text{pump}}X)\right]a_{\text{pump}} + i\kappa\varepsilon_{\text{pump}}(t), \quad (\text{S14})$$

$$\dot{a}_{\text{probe}} = -\left[\gamma_{\text{probe}} - i(\Delta_{\text{probe}} - g_{\text{probe}}X)\right]a_{\text{probe}} + i\kappa\varepsilon_{\text{probe}}(t), \quad (\text{S15})$$

$$\dot{X} = -\Gamma_m X + \Omega_m P, \quad (\text{S16})$$

$$\dot{P} = -\Gamma_m P - \Omega_m X + g_{\text{pump}}|a_{\text{pump}}|^2, \quad (\text{S17})$$

which describe the evolution of the pump and probe cavity modes and the mechanical mode. In the simulations, we considered a single mechanical eigenmode with frequency 26 MHz, similar to what was observed in our experiments. Here, Ω_m and Γ_m are the frequency and damping rate of the mechanical mode. Similar to our experiments, we chose the probe signal to be very weak, so that it does not induce mechanical or thermal oscillations. Consequently, the mechanical mode was induced only by the pump field as described by the expression in Eq. (S17). We see that this model explains our experimental observations well. In both the experimental results and the numerical simulations, it is clearly seen that the probe field follows the pump field during the bifurcation process.

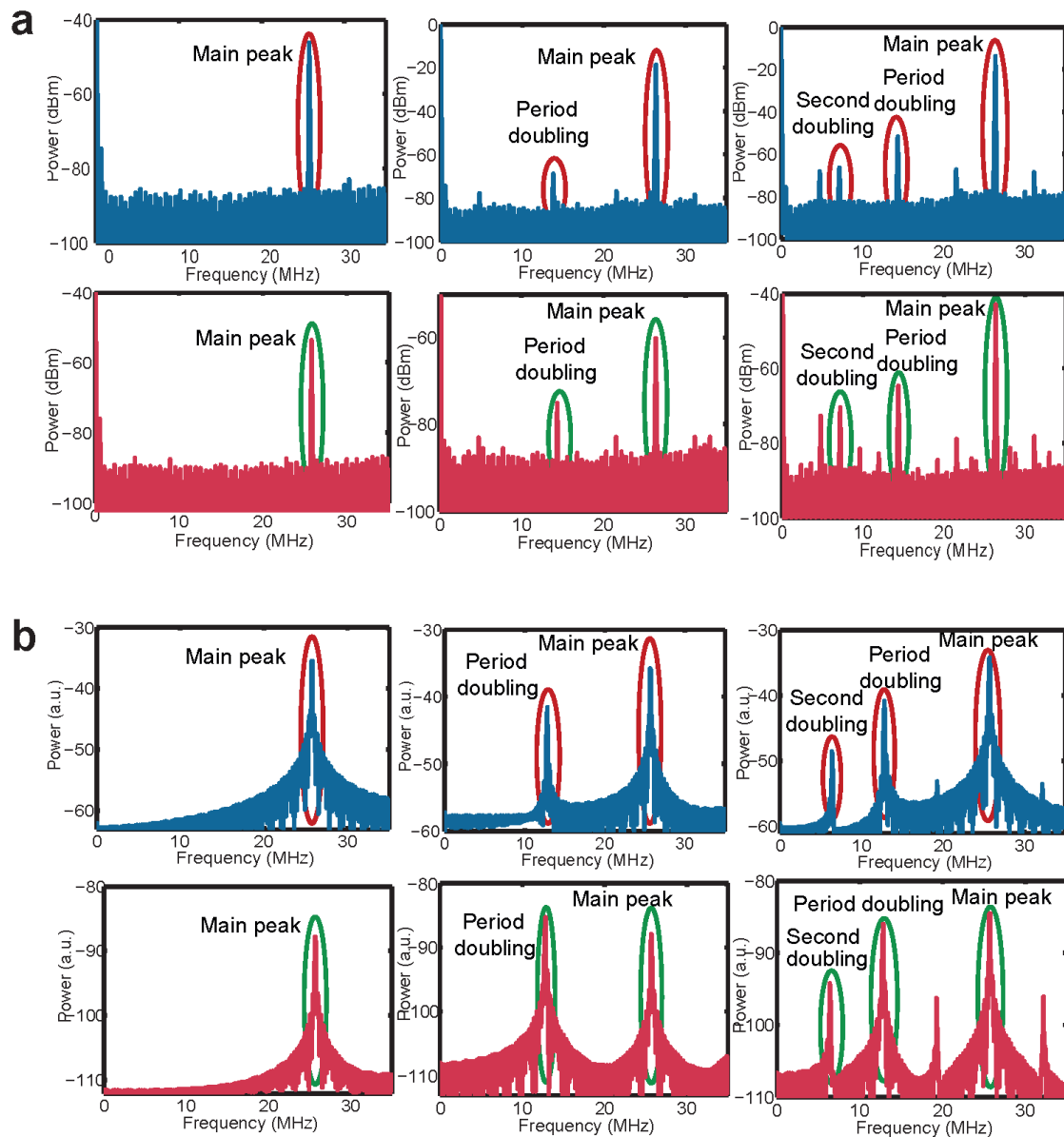


Figure S3. Optomechanically-induced period-doubling in the pump and probe fields. *a*, Experimental data and *b*, results of numerical simulations showing first and second period-doubling processes for the pump (red spectra) and probe (blue spectra) fields.

Our experimental data shown in Fig. S3a shows the existence of a second mechanical mode with frequency 5 MHz. This mode was excited when the pump power was increased to observe the second period-doubling process. Generally, one may think that this low-frequency mechanical mode would affect the bifurcation process of the 26 MHz mechanical mode, because these two mechanical modes are in the same micro-resonator and thus may couple to each other. But we could not see any signature of this in our experiments. We performed numerical simulations using COMSOL and found that the mechanical modes at 26 MHz and 5 MHz are, respectively, transverse and longitudinal modes (Fig.S4). Thus, they are orthogonal, which implies that there is minimal or no interaction between them.

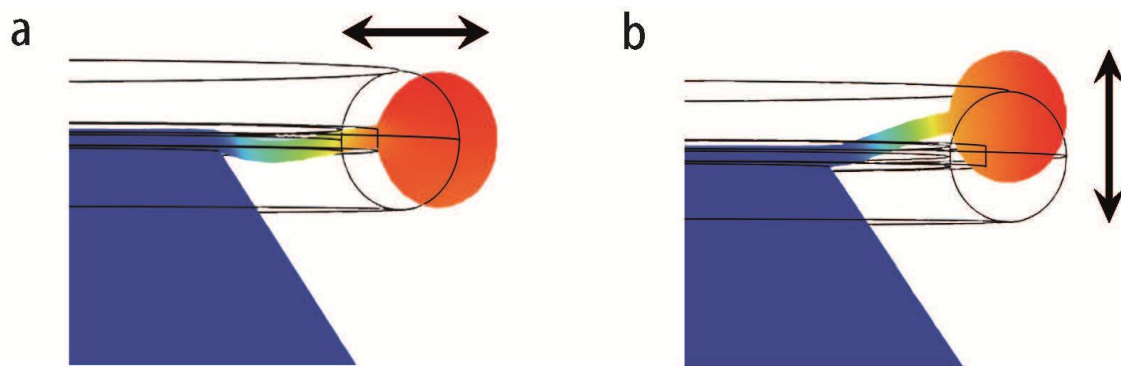


Figure S4. *Comsol simulation of the mechanical modes in a microtoroid. The mechanical mode with frequency a, 26 MHz is a transverse mode whereas the one with frequency b, 5 MHz is a longitudinal mode. Both of these mechanical modes were observed in our experiments, with the 5 MHz mode being excited only when the pump power was so high that the mode at 26 MHz experienced the second period doubling (Fig. S3). The orthogonality of these mechanical modes implies that there is no direct coupling between them.*

D. Optomechanically-induced optical nonlinearity for the probe field

In order to understand how the co-existence of the pump and probe fields in the same optomechanical resonator affect their interaction with the system and with each other, we consider the following Hamiltonian

$$H = \Delta_{\text{probe}} a_{\text{probe}}^\dagger a_{\text{probe}} + \varepsilon_{\text{probe}} (a_{\text{probe}}^\dagger + a_{\text{probe}}) + g_{\text{probe}} a_{\text{probe}}^\dagger a_{\text{probe}} X + \frac{\Omega_m}{2} (X^2 + P^2) \\ + \Delta_{\text{pump}} a_{\text{pump}}^\dagger a_{\text{pump}} + \kappa \varepsilon_{\text{pump}} (a_{\text{pump}}^\dagger + a_{\text{pump}}) + g_{\text{pump}} a_{\text{pump}}^\dagger a_{\text{pump}} X, \quad (\text{S18})$$

where the first (fourth) and second (fifth) terms are related to the free evolution of the probe (a_{probe} (pump a_{pump}) field, and the third (sixth) term explains the interaction of the probe (the pump) field with the mechanical mode X . The last term corresponds to the free evolution of the mechanical mode.

First, let us consider only the probe field by eliminating the fourth, fifth and sixth terms. In this case, we arrive at the Hamiltonian

$$H = \Delta_{\text{probe}} a_{\text{probe}}^\dagger a_{\text{probe}} + \kappa \varepsilon_{\text{probe}} (a_{\text{probe}}^\dagger + a_{\text{probe}}) + g_{\text{probe}} a_{\text{probe}}^\dagger a_{\text{probe}} X + \frac{\Omega_m}{2} (X^2 + P^2). \quad (\text{S19})$$

By introducing the translational transformation

$$\hat{X} = X + \frac{g_{\text{probe}}}{\Omega_m} a_{\text{probe}}^\dagger a_{\text{probe}}, \quad \hat{P} = P, \quad (\text{S20})$$

the Hamiltonian H can be re-expressed as [S1]

$$H = \Delta_{\text{probe}} a_{\text{probe}}^\dagger a_{\text{probe}} + \kappa \varepsilon_{\text{probe}} (a_{\text{probe}}^\dagger + a_{\text{probe}}) - \frac{g_{\text{probe}}^2}{2\Omega_m} (a_{\text{probe}}^\dagger a_{\text{probe}})^2 + \frac{\Omega_m}{2} (\hat{X}^2 + \hat{P}^2), \quad (\text{S21})$$

where we see that the nonlinear interaction between the probe field and the mechanical

motion leads to an effective Kerr-like nonlinearity in the optical mode a_{probe} , with its coefficient given as

$$\mu_{\text{probe}} = \frac{g_{\text{probe}}^2}{2\Omega_m}, \quad (\text{S22})$$

where Ω_m is the frequency of the mechanical mode. Equation (S22) implies that the optomechanically-induced Kerr-like nonlinearity is dependent on (i) the optomechanical coupling between the optical and mechanical modes and (ii) the frequency of the mechanical mode.

Following a similar procedure, we can derive the coefficient of nonlinearity for the case when only the pump field is present. In such a case, we have

$$H = \Delta_{\text{pump}} a_{\text{pump}}^\dagger a_{\text{pump}} + \kappa \varepsilon_{\text{pump}} (a_{\text{pump}}^\dagger + a_{\text{pump}}) + g_{\text{pump}} a_{\text{pump}}^\dagger a_{\text{pump}} X + \frac{\Omega_m}{2} (X^2 + P^2). \quad (\text{S23})$$

By introducing the transformation

$$\hat{X} = X + \frac{g_{\text{pump}}}{\Omega_m} a_{\text{pump}}^\dagger a_{\text{pump}}, \quad \hat{P} = P, \quad (\text{S24})$$

we rewrite the Hamiltonian as

$$H = \Delta_{\text{pump}} a_{\text{pump}}^\dagger a_{\text{pump}} + \kappa \varepsilon_{\text{pump}} (a_{\text{pump}}^\dagger + a_{\text{pump}}) - \frac{g_{\text{pump}}^2}{2\Omega_m} (a_{\text{pump}}^\dagger a_{\text{pump}})^2 + \frac{\Omega_m}{2} (\hat{X}^2 + \hat{P}^2). \quad (\text{S25})$$

Thus, the coefficient of the effective Kerr-like nonlinearity in the optical mode a_{pump} becomes

$$\mu_{\text{pump}} = \frac{g_{\text{pump}}^2}{2\Omega_m}, \quad (\text{S26})$$

where Ω_m is the frequency of the mechanical mode and g_{pump} is the strength of the coupling between the pump and mechanical modes.

Now let us consider the case where both the pump and probe fields exist within the same resonator and they are coupled to the same mechanical mode. In this case, by applying the transformation

$$\tilde{X} = X + \frac{g_{\text{probe}}}{\Omega_m} a_{\text{probe}}^\dagger a_{\text{probe}} + \frac{g_{\text{pump}}}{\Omega_m} a_{\text{pump}}^\dagger a_{\text{pump}}, \quad \tilde{P} = P, \quad (\text{S27})$$

we re-express the Hamiltonian given in Eq. (S18) as

$$\begin{aligned} H = & \Delta_{\text{probe}} a_{\text{probe}}^\dagger a_{\text{probe}} + \kappa \varepsilon_{\text{probe}} (a_{\text{probe}}^\dagger + a_{\text{probe}}) - \frac{g_{\text{probe}}^2}{2\Omega_m} (a_{\text{probe}}^\dagger a_{\text{probe}})^2 + \frac{\Omega_m}{2} (\tilde{X}^2 + \tilde{P}^2) \\ & + \Delta_{\text{pump}} a_{\text{pump}}^\dagger a_{\text{pump}} + \kappa \varepsilon_{\text{pump}} (a_{\text{pump}}^\dagger + a_{\text{pump}}) - \frac{g_{\text{pump}}^2}{2\Omega_m} (a_{\text{pump}}^\dagger a_{\text{pump}})^2 - \frac{g_{\text{pump}} g_{\text{probe}}}{\Omega_m} (a_{\text{probe}}^\dagger a_{\text{probe}}) (a_{\text{pump}}^\dagger a_{\text{pump}}). \end{aligned} \quad (\text{S28})$$

Here the third and seventh terms are the coefficients of the Kerr-like nonlinearity derived earlier for the cases when only the probe or the pump fields exist in the optomechanical resonator. The last term, on the other hand, is new and implies an effective interaction between the pump and probe fields, if they both exist in the optomechanical resonator.

The dynamical equations of this system can be written as

$$\dot{a}_{\text{pump}} = -\left[\gamma_{\text{pump}} - i(\Delta_{\text{pump}} - g_{\text{pump}} X)\right] a_{\text{pump}} + i\kappa \varepsilon_{\text{pump}}, \quad (\text{S29})$$

$$\dot{a}_{\text{probe}} = -\left[\gamma_{\text{probe}} - i(\Delta_{\text{probe}} - g_{\text{probe}} X)\right] a_{\text{probe}} + i\kappa \varepsilon_{\text{probe}}. \quad (\text{S30})$$

In the long-time limit (i.e., steady-state), we have $\dot{a}_{\text{pump}}, \dot{a}_{\text{probe}} \approx 0$, which leads to

$$a_{\text{probe}} = \frac{i\kappa\mathcal{E}_{\text{probe}}}{\gamma_{\text{probe}} - i(\Delta_{\text{probe}} - \mathcal{G}_{\text{probe}}X)} \approx \frac{i\kappa\mathcal{E}_{\text{probe}}}{\gamma_{\text{probe}} - i\Delta_{\text{probe}}} + \frac{\kappa\mathcal{E}_{\text{probe}}\mathcal{G}_{\text{probe}}}{(\gamma_{\text{probe}} - i\Delta_{\text{probe}})^2} X, \quad (\text{S31})$$

$$a_{\text{pump}} = \frac{i\kappa\mathcal{E}_{\text{pump}}}{\gamma_{\text{pump}} - i(\Delta_{\text{pump}} - \mathcal{G}_{\text{pump}}X)} \approx \frac{i\kappa\mathcal{E}_{\text{pump}}}{\gamma_{\text{pump}} - i\Delta_{\text{pump}}} + \frac{\kappa\mathcal{E}_{\text{pump}}\mathcal{G}_{\text{pump}}}{(\gamma_{\text{pump}} - i\Delta_{\text{pump}})^2} X. \quad (\text{S32})$$

If we further eliminate the degrees of freedom of the mechanical mode X from the above equations, then, under the conditions that $\gamma_{\text{pump}} = \gamma_{\text{probe}}$, $\Delta_{\text{pump}} = \Delta_{\text{probe}}$, and $\mathcal{G}_{\text{pump}} = \mathcal{G}_{\text{probe}}$, we have

$$a_{\text{pump}} = (\mathcal{E}_{\text{pump}}/\mathcal{E}_{\text{probe}}) a_{\text{probe}}. \quad (\text{S33})$$

By substituting this equation into the last term in Eq. (S28), we see that the last term of the Hamiltonian becomes

$$\frac{\mathcal{G}_{\text{pump}}\mathcal{G}_{\text{probe}}}{\Omega_m} (a_{\text{probe}}^\dagger a_{\text{probe}})(a_{\text{pump}}^\dagger a_{\text{pump}}) \rightarrow \frac{\mathcal{G}_{\text{pump}}\mathcal{G}_{\text{probe}}\mathcal{E}_{\text{pump}}^2}{\Omega_m \mathcal{E}_{\text{probe}}^2} (a_{\text{probe}}^\dagger a_{\text{probe}})^2, \quad (\text{S34})$$

from which we define the coefficient of nonlinearity as

$$\tilde{\mu}_{\text{probe}} = \frac{\mathcal{G}_{\text{probe}}^2 \mathcal{E}_{\text{pump}}^2}{\Omega_m \mathcal{E}_{\text{probe}}^2}. \quad (\text{S35})$$

It is clear that even a very weak probe field can experience a strong Kerr nonlinearity, and hence a nonlinear dynamics, if the intensity of the pump is sufficiently strong. Thus, our experimental system intrinsically enables an optomechanically-induced Kerr-like nonlinearity, which helps the optical pump and probe fields interact with each other. It is clear that the strength of the interaction can be made very high by increasing the ratio of the intensity of the input pump field $\mathcal{E}_{\text{pump}}^2$ to that of the input probe field $\mathcal{E}_{\text{probe}}^2$. In our experiments, the pump field is at least three-

orders of magnitude larger than the probe field. Thus the nonlinear coefficient $\tilde{\mu}_{\text{probe}}$ given in Eq. (S35) is increased by at least three-orders of magnitude, compared to the nonlinear coefficient μ_{probe} given in Eq. (S22).

E. Reconstructing the mechanical motion

Here we explain our method used to estimate the trajectory of the mechanical motion from the experimentally-available data. The mechanical mode excited in our microtoroid during the experiments had a frequency of $\Omega_m = 26.1$ MHz and a damping rate of $\Gamma_m = 0.2$ MHz, implying a quality factor of $Q_m \approx 130$. We used these values in the nonlinear optomechanical equations to reconstruct the mechanical motion. We found that the optomechanical resonator experiences a periodic motion (Fig. S5a) even when the detected optical pump field showed chaotic behavior. To explain this, we start from the following equation for the mechanical resonator

$$\dot{X} = -\Gamma_m X + \Omega_m P, \quad (\text{S36})$$

$$\dot{P} = -\Gamma_m P - \Omega_m X + g_{\text{pump}} I(t), \quad (\text{S37})$$

where P is the momentum of the mechanical mode and $I(t) = |a_{\text{pump}}(t)|^2$ is the intensity of the pump with the field amplitude a_{pump} . By introducing the complex amplitude $b = (X + iP)/\sqrt{2}$, Eqs. (S36) and (S37) can be rewritten as

$$\dot{b} = -(\Gamma_m - i\Omega_m)b + g_{\text{pump}} I(t). \quad (\text{S38})$$

The above equation can be solved in the frequency domain as

$$b(\omega) = \frac{\mathcal{G}_{\text{pump}}}{i(\omega - \Omega_m) + \Gamma_m} I(\omega), \quad (\text{S39})$$

from which we obtain

$$S_b(\omega) = |b(\omega)|^2 = \frac{\mathcal{G}_{\text{pump}}^2}{(\omega - \Omega_m)^2 + \Gamma_m^2} |I(\omega)|^2 = \frac{\mathcal{G}_{\text{pump}}^2}{\Gamma_m^2} \chi_{bl}(\omega) S_I(\omega), \quad (\text{S40})$$

where

$$\chi_{bl}(\omega) = \frac{\Gamma_m^2}{(\omega - \Omega_m)^2 + \Gamma_m^2} \quad (\text{S41})$$

is the susceptibility coefficient induced by the mechanical resonator and $S_I(\omega) = |I(\omega)|^2$ is the spectrum of $I(t)$. As shown in Fig. S5a, the mechanical resonator works similar to a low-pass filter, which filters out the high-frequency components of $I(t)$. In fact, the susceptibility coefficient $\chi_{bl}(\omega)$ modifies the shape of $S_I(\omega)$ and shrinks the spectrum $S_b(\omega)$ to the low-frequency regime. By such a filtering process, the mechanical motion of the resonator does not experience the high-frequency components typical of chaotic behavior, but instead remains in the periodic-oscillation regime, as shown in the reconstructed motion of the mechanical mode in Fig. S5b.

F. Effect of system parameters on the maximum Lyapunov exponent

Lyapunov exponents quantify sensitivity of a system to initial conditions and give a measure of predictability. They are a measure of the rate of convergence or divergence of nearby trajectories. A positive exponent implies divergence and that the orbits are on a chaotic attractor.

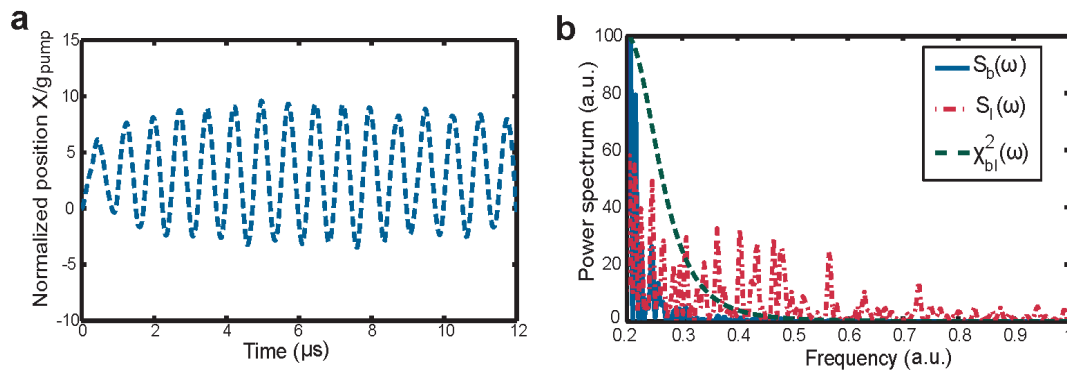


Figure S5. Reconstructed mechanical motion of the microtoroid resonator. a, Periodic mechanical motion of the microtoroid when the pump and probe fields are both in the chaotic regime. **b,** Filtering by the mechanical resonator: the mechanical resonator works as a low-pass filter which filters out the high-frequency components in the mechanical modes.

A negative exponent implies convergence to a common fixed point. Zero exponent implies that the orbits maintain their relative positions and they are on a stable attractor. In the main text of the manuscript, we presented the experimental results which show how the pump power affects the maximum Lyapunov exponent of the pump and probe fields. Here, we present numerical results (Fig. S6) regarding the effect of the frequency detuning between the cavity resonance and the pump, frequency detuning between the cavity resonance and the probe, and the damping rates of the pump and probe on the maximum Lyapunov exponent. As seen in Fig. S6a, Lyapunov exponents of the pump and probe fields vary with increasing frequency detuning between the pump and the cavity resonance. As the frequency detuning of the pump increases, Lyapunov exponent increases from negative to positive values, attaining its maximum value at a detuning value of $\Delta_{\text{pump}} \approx 0.9 \Omega_m$, which coincides well with the numerical results in Ref. [S2]. Further increase of detuning, decreases the maximum Lyapunov exponent which becomes negative.

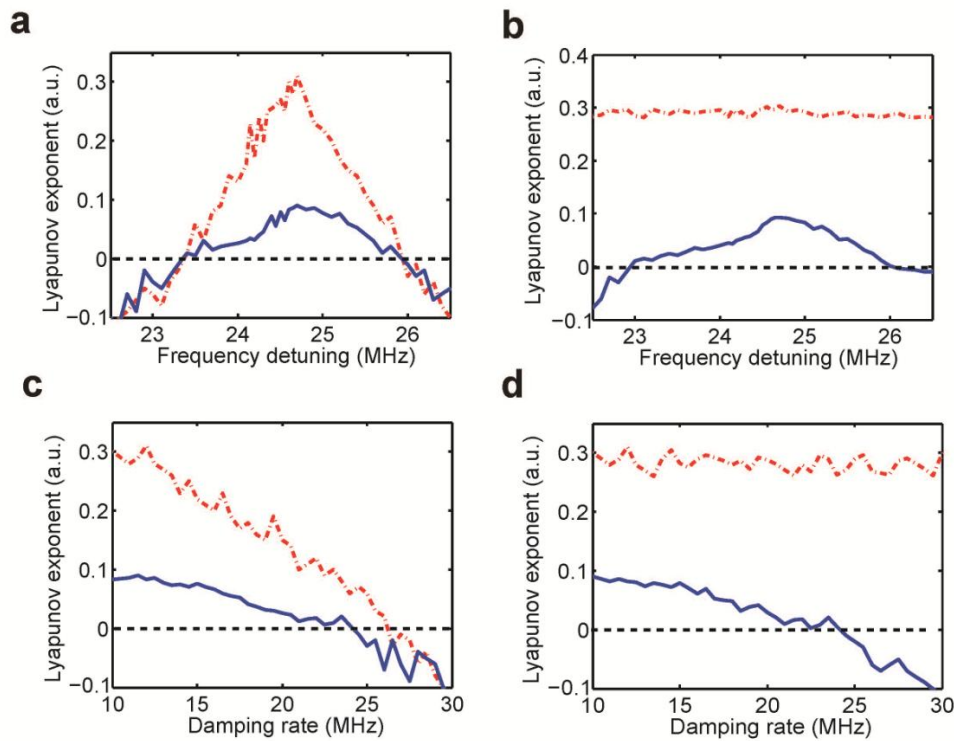


Figure S6. Maximum of the Lyapunov exponent for the pump (red spectra) and probe (blue spectra) fields. Effect of the (a) pump-cavity detuning, (b) probe-cavity detuning, (c) damping rate of the pump, and (d) damping rate of the probe on the maximum Lyapunov exponents of the pump and probe fields.

Thus, with increasing detuning of the pump from the cavity resonance, the system evolves first to chaotic regime and then gets out of chaos into a periodic dynamics. This is similar to the behavior observed for the varying pump field. Interestingly, both the pump and probe fields follow the same dependence on the pump-cavity detuning. When we look at the effect of probe-cavity detuning (Fig. S6b), we see that varying probe-cavity detuning affects only the maximum Lyapunov exponent of the probe, and the pump Lyapunov exponent is not affected. The reason

for this is that in our experiments and in these simulations, we kept the power of the probe field so weak that it does not affect the pump field. A similar trend is seen in the case of varying the damping rates of the pump and probe modes, that is varying the damping rate of the pump affects Lyapunov exponents of both the pump and probe (Fig. S6c) but varying the damping rate of the probe affects only the Lyapunov exponent of the probe (Fig. S6d). In Fig. S6c that with increasing damping rate the maximum Lyapunov exponent decreases from a positive value down to negative values. This can be explained as follows. Increasing damping rate, decreases the quality factor of resonator which in turn reduces the intracavity field intensity. As a result optomechanical oscillation is gradually suppressed and the degree of the chaos induced by optomechanical interaction decreases.

G. Derivation of the fitting curve for SNR in stochastic resonance

To obtain more insight into the stochastic resonance phenomenon, let us first focus on the dynamics of the optical mode coupled to the probe field a_{probe} . The total Hamiltonian of the optical modes a_{pump} , a_{probe} , and the mechanical mode can be written as in Eq. (S18). By introducing the translation transformation in Eq. (S27) and getting rid of the degrees of freedom of the mechanical mode and the optical mode coupled to the pump field a_{pump} , the Hamiltonian in Eq. (S18) can be re-expressed as

$$H = \Delta_{\text{probe}} a_{\text{probe}}^\dagger a_{\text{probe}} + \kappa \varepsilon_{\text{probe}} (a_{\text{probe}}^\dagger + a_{\text{probe}}) - \tilde{\mu}_{\text{probe}} (a_{\text{probe}}^\dagger a_{\text{probe}})^2, \quad (\text{S42})$$

where $\tilde{\mu}_{\text{probe}}$ is given in Eq. (S35). We can see that the nonlinear optomechanical coupling leads

to an effective fourth-order nonlinear term in the optical mode a_{probe} . Introducing the normalized position and momentum operators

$$x_{\text{probe}} = \frac{1}{\sqrt{2}}(a_{\text{probe}}^\dagger + a_{\text{probe}}), \quad p_{\text{probe}} = \frac{i}{\sqrt{2}}(a_{\text{probe}}^\dagger - a_{\text{probe}}), \quad (\text{S43})$$

we write the following dynamical equation by dropping some non-resonant terms and introducing the noise terms:

$$\dot{x}_{\text{probe}} = -\gamma_{\text{probe}}x_{\text{probe}} + \omega_{\text{probe}}p_{\text{probe}}, \quad (\text{S44})$$

$$\dot{p}_{\text{probe}} = -\Delta_{\text{probe}}x_{\text{probe}} - \gamma_{\text{probe}}p_{\text{probe}} + \tilde{\mu}_{\text{probe}}x_{\text{probe}}^3 + \kappa\varepsilon_{\text{probe}}(t) + \xi(t), \quad (\text{S45})$$

where $\xi(t)$ is a noise term with a correlation time negligibly small when compared to the characteristic time scale of the optical modes and mechanical mode of the optomechanical resonator:

$$\langle \xi(t)\xi(t') \rangle = 2D\delta(t-t'), \quad (\text{S46})$$

with D denoting the strength of the noise. Subsequently, we arrive at the second-order oscillation equation

$$\ddot{x}_{\text{probe}} + 2\gamma_{\text{probe}}\dot{x}_{\text{probe}} = -(\Delta_{\text{probe}}^2 + \gamma_{\text{probe}}^2)x_{\text{probe}} + \tilde{\mu}_{\text{probe}}\Delta_{\text{probe}}x_{\text{probe}}^3 + \kappa\Delta_{\text{probe}}\varepsilon_{\text{probe}}(t) + \Delta_{\text{probe}}\xi(t). \quad (\text{S47})$$

Under the condition that $\Delta_{\text{probe}} \ll \gamma_{\text{probe}}$ in the overdamped limit, the above second-order oscillation equation can be reduced to

$$\dot{x}_{\text{probe}} = -\frac{\Delta_{\text{probe}}^2}{2\gamma_{\text{probe}}}x_{\text{probe}} + \tilde{\mu}_{\text{probe}}\frac{\Delta_{\text{probe}}}{2\gamma_{\text{probe}}}x_{\text{probe}} + \kappa\frac{\Delta_{\text{probe}}}{2\gamma_{\text{probe}}}\varepsilon_{\text{probe}}(t) + \frac{\Delta_{\text{probe}}}{2\gamma_{\text{probe}}}\xi(t). \quad (\text{S48})$$

If we introduce the normalized time unit $\tau = (2\gamma_{\text{probe}}/\Delta_{\text{probe}})t$, we arrive at

$$\frac{d}{d\tau} x_{\text{probe}} = -\Delta_{\text{probe}} x_{\text{probe}} + \tilde{\mu}_{\text{probe}} x_{\text{probe}}^3 + \kappa \varepsilon_{\text{probe}}(\tau) + \xi(\tau). \quad (\text{S49})$$

which is a typical equation leading to the stochastic resonance phenomenon [S3], [S4], [S5].

The signal-to-noise ratio (SNR) for such a system is given by

$$\text{SNR} = \frac{\Delta_{\text{probe}}^2 \Omega_m^2 \kappa^2 \varepsilon_{\text{probe}}^2}{8\sqrt{2} D^2 g_{\text{probe}}^4} \exp\left(-\frac{\Delta_{\text{probe}}^2 \Omega_m}{8g_{\text{probe}}^2 D}\right). \quad (\text{S50})$$

Since the strength of the noise D is related to the pump power P_{pump} by $D = \alpha P_{\text{pump}}^{1/2}$, the relation

between the SNR and the pump power can be re-written as

$$\text{SNR} = \frac{\Delta_{\text{probe}}^2 \Omega_m^2 \kappa^2 \varepsilon_{\text{probe}}^2}{8\sqrt{2} \alpha^2 P_{\text{pump}} g_{\text{probe}}^4} \exp\left(-\frac{\Delta_{\text{probe}}^2 \Omega_m}{8g_{\text{probe}}^2 \alpha P_{\text{pump}}}\right), \quad (\text{S51})$$

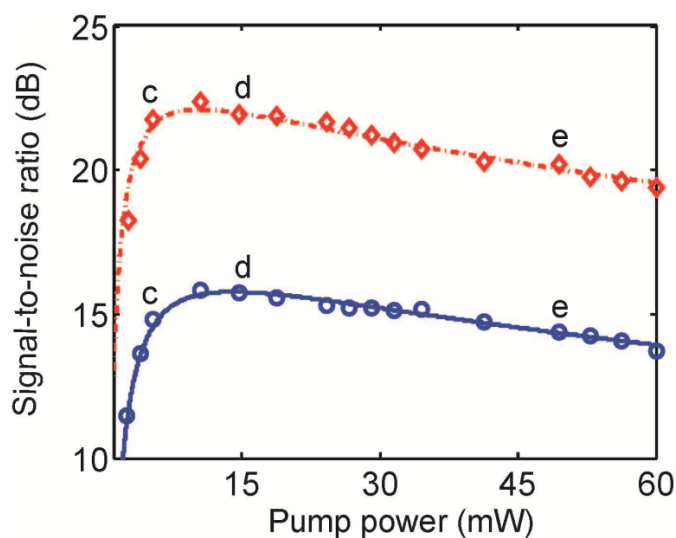


Figure S7. Signal-to-noise ratio (SNR) for the pump and probe signals. Experimentally-obtained signal-to-noise ratio (SNR) of the probe (blue open circles) and pump (red diamonds) signals as a function of the pump power. Solid curves are the best fits to the experimental data.

which implies that the SNR is not a monotonous function of the pump power P_{pump} and hence it is possible to increase the SNR by increasing the pump power (i.e., subsequently by increasing the bandwidth D and hence the noise). Following the same procedure one can derive SNR for the pump in a straightforward way.

In Figure S7, we give the SNR versus pump power for both the probe and pump fields measured in our experiments together with the best fit according to Eq. (S51) for the probe and the similar expression for the pump. Keeping ε and β as free parameters, we found the best fits with $\varepsilon = 0.825$ mW and $\beta = 7.4764$ mW^{1/2} for the probe and with $\varepsilon = 2.6388$ mW and $\beta = 6.47$ mW^{1/2} for the pump.

H. Stochastic resonance or coherence resonance?

Stochastic resonance is a phenomenon in which the response of a nonlinear system to a weak input signal is optimized by the presence of a particular level of noise, i.e., the noise-enhanced response of a deterministic input signal [S3]. Coherence resonance is a related effect demonstrating the constructive role of noise, and is known as stochastic resonance without input signal. Coherence resonance helps to improve the temporal regularity of a bursting time series signal [S7]. The main difference between stochastic resonance and coherence resonance is whether a deterministic input signal is input to the system and whether the induced SNR enhancement is the consequence of the response of this deterministic input signal [S15]. In our system, a weak probe signal, which is modulated by the mechanical mode of the optomechanical resonator at the frequency $\Omega_m = 26$ MHz, acts as a periodic input signal fed into the system.

In order to confirm that the observed phenomenon in our experiments is stochastic resonance rather than coherence resonance, we performed numerical simulations and compared the results

with our experimental results. The dynamical equations we use for numerical simulation are given by

$$\dot{a}_{\text{pump}} = -\left[\gamma_{\text{pump}} - i(\Delta_{\text{pump}} - g_{\text{pump}}X)\right]a_{\text{pump}} + i\kappa\varepsilon_{\text{pump}}(t) + D_{\text{pump}}\xi_{\text{pump}}(t), \quad (\text{S52})$$

$$\dot{a}_{\text{probe}} = -\left[\gamma_{\text{probe}} - i(\Delta_{\text{probe}} - g_{\text{probe}}X)\right]a_{\text{probe}} + i\kappa\varepsilon_{\text{probe}}(t) + D_{\text{probe}}\xi_{\text{probe}}(t), \quad (\text{S53})$$

$$\dot{X} = -\Gamma_m X + \Omega_m P, \quad (\text{S54})$$

$$\dot{P} = -\Gamma_m P - \Omega_m X + g_{\text{pump}}|a_{\text{pump}}|^2 + D_m \xi_m(t), \quad (\text{S55})$$

with parameters $\Delta_{\text{pump}}/\Omega_m = \Delta_{\text{probe}}/\Omega_m = 1$, $\gamma_{\text{pump}}/\Delta_{\text{pump}} = 0.1$, $\gamma_{\text{probe}}/\Delta_{\text{probe}} = 0.1$, $\Gamma_m/\Omega_m = 0.01$, $g_{\text{pump}}/\Delta_{\text{pump}} = g_{\text{probe}}/\Delta_{\text{probe}} = 0.1$, $\kappa/\Delta_{\text{pump}} = \varepsilon_{\text{pump}}/\Delta_{\text{pump}} = 1$, $D_{\text{pump}}/\Delta_{\text{pump}} = 0.1$, $D_{\text{probe}}/\Delta_{\text{probe}} = 0.1$, $D_m/\Omega_m = 0.1$. $\xi_{\text{pump}}(t)$, $\xi_{\text{probe}}(t)$, $\xi_m(t)$ are white noises such that

$$E[\xi_i(t)] = 0, E[\xi_i(t)\xi_j(t')] = \delta_{ij}\delta(t-t'), \quad (\text{S56})$$

where $E(\cdot)$ is average over the noise. In the case of stochastic resonance, we set $\varepsilon_{\text{probe}}/\Delta_{\text{probe}} = 0.1$, and in the case of coherence resonance we set $\varepsilon_{\text{probe}}/\Delta_{\text{probe}} = 0$, to simulate the system with a weak probe input and without the weak probe input, respectively. First, we compare the output spectra obtained in our experiments (Fig. S8a) with the results of numerical simulations where in our theoretical model introduced in the previous section is considered with and without weak probe input to simulate stochastic resonance (Fig. S8b) and coherence resonance (Fig. S8c). We see that in the output spectra obtained in the experiments (Fig. S8a) and the simulations with weak probe input (Fig. S8b), the position of the resonant peaks are not affected by increasing pump power. The spectral position of the resonant peak in the output spectra is fixed at the frequency of the periodic input signal. However, for the case, with no weak

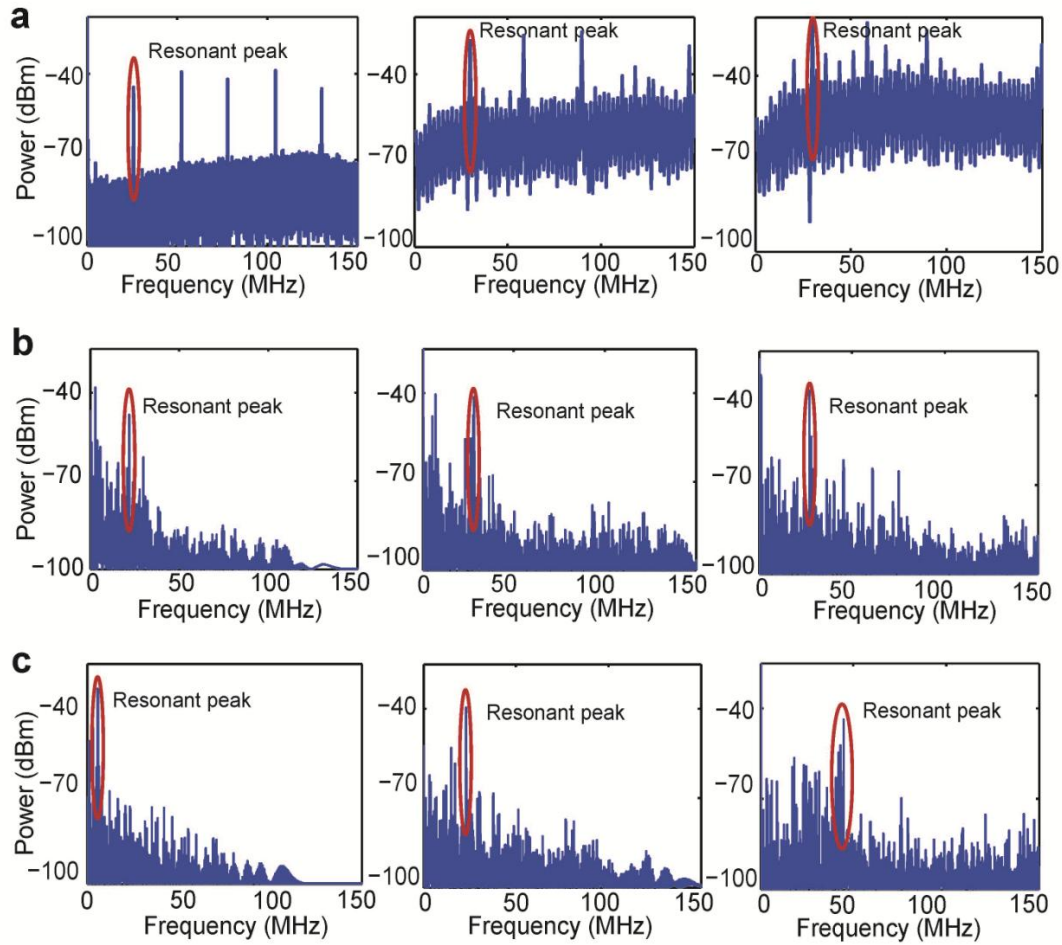


Figure S8. Output spectra obtained in the experiments and in the numerical simulations of stochastic resonance and coherence resonance at various pump powers. **a**, Output spectra obtained in the experiments show that the spectral location of the resonance peak do not change with increasing pump power. **b**, Output spectra obtained in the numerical simulations of stochastic resonance show that the spectral location of the resonance peak stays the same for increasing pump power, similar to what was observed in the experiments. **c**, Output spectra obtained in the numerical simulations of coherence resonance which show that the spectral location of the resonance peaks change with increasing pump power. From left to the right, the input pump power is increased.

probe input, simulating coherence resonance, the positions of the resonant peaks in the output spectra shift with increasing pump power, implying that the resonances are induced by noise [S13] Thus, the behavior of the resonances in the output spectra obtained in the experiments agrees with what one would expect for stochastic resonance, and it is completely different that what one would expect for coherence resonance.

Next, we compare the mean interspike intervals and its scaled standard deviation calculated from the output signal measured in our experiments with the results of numerical simulations of our system when a weak probe field is used as an input (case of stochastic resonance) and when there is no input probe field (case of coherence resonance). The interspike interval is defined as the mean time between two adjacent spikes in the time-domain output signals [S14] ,

$$\langle \tau \rangle = \lim_{N \rightarrow \infty} \frac{1}{N} \sum_{i=1}^N \tau_i, \quad (\text{S.57})$$

where τ_i is the time between the i -th and $(i+1)$ -th spikes. The variation R of the interspike intervals which is defined as the scaled standard deviation of the mean interspike interval is given as [S14]

$$R = \frac{\sqrt{\langle \tau^2 \rangle - \langle \tau \rangle^2}}{\langle \tau \rangle}. \quad (\text{S.58})$$

In Fig. S9, we present the results of experiments (Fig. S9a) and the numerical simulations for stochastic resonance (Fig. S9b) and for coherence resonance (Fig. S9c). The pump power dependence of $\langle \tau \rangle$ and R obtained for our experimental data and that obtained for the numerical simulation of stochastic resonance agree well, that is in both the experiments and numerical simulations we see that pump power does not affect $\langle \tau \rangle$ much, and R reaches a maximum at an optimal pump power (i.e., R is a concave). From the results of the simulations

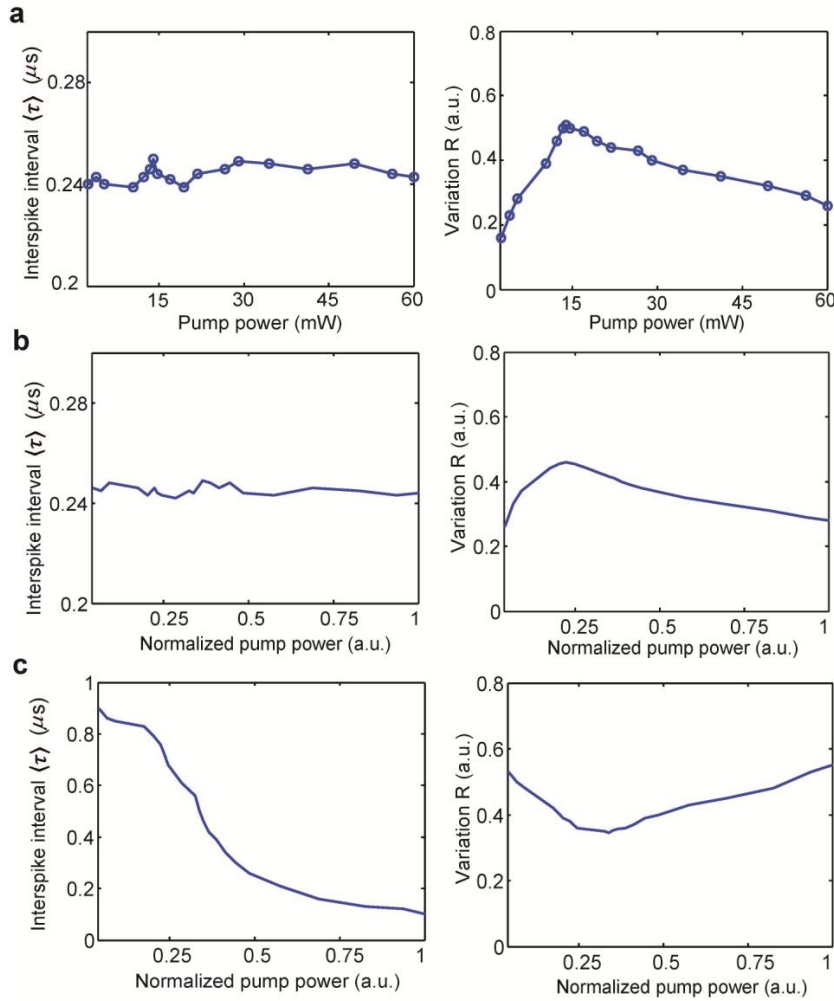


Figure S9. Mean interspike interval and its variation for the probe mode. a, Mean interspike interval and its variation calculated from the output signal in the probe mode obtained in the experiments. **b,** Mean interspike interval and its variation obtained in the numerical simulation of stochastic resonance in our system (with input weak probe). **c,** Mean interspike interval and its variation obtained in the numerical simulation of coherence resonance in our system (without input weak probe). Experimental results agree well with the simulation results of stochastic resonance, and demonstrate a completely different dynamics than the coherence resonance. This imply that the observed phenomenon in the experiments is stochastic resonance.

of coherence resonance, we see that (i) the mean interspike interval $\langle \tau \rangle$ drops gradually with increasing pump power, and (ii) R is a concave function, exhibiting a minimum at an optimal pump power [S16]. The very good agreement between what we have observed in the experiments and the results of the numerical simulations of stochastic resonance in the theoretical model describing our system strongly supports that what we have observed in the experiments is stochastic resonance rather than coherence resonance.

References:

- [S1] Gong, Z. R., Ian, H., Liu, Y.-X., Sun, C. P. & Nori, F. Effective Hamiltonian approach to the Kerr nonlinearity in an optomechanical system. *Phys. Rev. A* **80**, 065801 (2009).
- [S2] Bakemeier, L., Alvermann, A. & Fehske, H. Route to chaos in optomechanics. *Phys. Rev. Lett.* **114**, 336 013601 (2014).
- [S3] Gammaitoni, L., Hänggi, P., Jung, P. & Marchesoni, F. Stochastic Resonance. *Rev. Mod. Phys.* **70**, 223-287 (1998).
- [S4] McNamara, B., Wiesenfeld K. & Roy, R. Observation of stochastic resonance in a ring laser. *Phys. Rev. Lett.* **60**, 2626-2629 (1988).
- [S5] Gammaitoni, L., Marchesoni, F., Menichella-Saetta, E. & Santucci, S. Stochastic resonance in bistable systems. *Phys. Rev. Lett.* **62**, 349-352 (1989).
- [S6] Anishchenko, V. S., Neiman, A. B. & Safanova, M. A. Stochastic resonance in chaotic systems. *J. Stat. Phys.* **70**, 183-196 (1993).
- [S7] Liu Z. & Lai Y.-C. Coherence resonance in coupled chaotic oscillators. *Phys. Rev. Lett.* **86**, 4737-4740 (2001).
- [S8] Karsaklian Dal Bosco, A., Wolfersberger D. & Sciamanna, M. Delay-induced

- deterministic resonance of chaotic dynamics. *Euro. Phys. Lett.* **101**, 24001 (2013).
- [S9] Pikovsky A. S. & Kurths, J. Coherence resonance in a noise-driven excitable system. *Phys. Rev. Lett.* **78**, 775-778 (1997).
- [S10] C. Masoller, Noise-induced resonance in delayed feedback systems. *Phys. Rev. Lett.* **88**, 034102 (2002).
- [S11] Arizaleta Arteaga, M., Valencia, M., Sciamanna, M., Thienpont, H., Lopez-Amo, M. & Panajotov, K. Experimental evidence of coherence resonance in a time-delayed bistable system. *Phys. Rev. Lett.* **99**, 023903 (2007).
- [S12] Neiman, A., Sapsin, P. I. & Stone, L. Coherence resonance at noisy precursors of bifurcations in nonlinear dynamical systems. *Phys. Rev. E* **56**, 270-273 (1997).
- [S13] Gang, H., Ditzinger, T., Ning, C. Z. & Haken, H. Stochastic resonance without external periodic force. *Phys. Rev. Lett.* **71**, 807 (1993).
- [S14] Lindner B. & Schimansky-Geier L. Analytical approach to the stochastic FitzHugh-Nagumo system and coherence resonance. *Phys. Rev. E* **60**, 7270-7276 (1999).
- [S15] Sagués, F., Sancho, J. M. & García-Ojalvo, J. Spatiotemporal order out of noise. *Rev. Mod. Phys.* **79**, 829-882 (2007).
- [S16] Lemarchand, A., Gorecki, J., Gorecki, A. & Nowakows, B. Temperature-driven coherence resonance and stochastic resonance in a thermochemical system. *Phys. Rev. E* **89**, 022916 (2014).